4

Second Order Shear Deformation Theory (SSDT) for Free Vibration Analysis on a Functionally Graded Quadrangle Plate

A. Shahrjerdi[1] and F. Mustapha[2]
[1]*Department of Mechanical Engineering, Malayer University, Malayer,*
[2]*Department of Aerospace Engineering, Universiti Putra Malaysia,*
43400 UPM, Serdang, Selangor
[1]*Iran*
[2]*Malaysia*

1. Introduction

Studies of vibration of plates have matured and are a well-established branch of research in structural dynamics. They have a vast range of applications in engineering and technology. But not much work can be found on vibration analysis of Functionally Graded Materials (FGMs) as compared to isotropic and composite plates and shells. FGMs are those in which the volume fraction of the two or more constituent materials is varied, as a power-law distribution, continuously as a function of position along certain dimension(s) of the structure [1, 2].
From the perspective of finite element method (FEM) studies of FGM, Praveen and Reddy [3], studied the static and dynamic responses of functionally graded (FG) ceramic-metal plate accounting for the transverse shear deformation, rotary inertia and moderately large rotations in the Von-Karman sense, in which the effect of an imposed temperature field on the response of the FG plate was discussed in detail. Ng et al. [4] dealt with the parametric resonance of FG rectangular plates under harmonic in-plane loading. Ferreira and Batra [5] provided a global collocation method for natural frequencies of FG plates by a meshless method with first order shear deformation theory (FSDT). Woo et al. [6] presented an analytical solution for the nonlinear free vibration behavior of FGM plates, where the fundamental equations were obtained using the Von-Karman theory for large transverse deflection, and the solution was based in terms of mixed Fourier series. Zhao et al. [7] studied the free vibration analysis of metal and ceramic FG plates using the element-free kp-Ritz method. The FSDT was employed to account for the transverse shear strain and rotary inertia, mesh-free kernel particle functions were used to approximate the two-dimensional displacement fields and the eigen-equation was obtained by applying the Ritz procedure to the energy functional of the system. Batra and Jin [8] used the FSDT coupled with the FEM to study the free vibrations of an FG anisotropic rectangular plate with various edge conditions. Also, Batra and Aimmanee [9] studied a higher order shear and normal deformable plate theory by FEM. Many studies conducted on FGMs are related to the analysis of free vibration by applying FSDT (see [10-12] and the references there in).
Other forms of shear deformation theory, such as the third order-shear deformation theory (TSDT) that accounts for the transverse effects, have been considered. Cheng and Batra [13]

applied Reddy's third order plate theory to study buckling and steady state vibrations of a simply supported FG isotropic polygonal plate [14]. Vel and Batra [14] dealt with the three-dimensional exact solution for free and forced vibrations of simply supported FGM rectangular plates using FDST and TSDT by employing the power series method. Nonlinear vibration and dynamic response of FGM plates in thermal environments were studied by Huang et al. [15] based on the higher-order shear deformation plate theory and general Von-Karman type equation. Static analysis of FG plates using TSDT and a meshless method were also presented by Ferreira et al. [16].

As for the first-order shear deformation plate theory (FSDT), the theory extends the kinematics of the classical plate theory (CPT) by relaxing the normality restriction and allowing for arbitrary but constant rotation of transverse normals. On the other hand, the second and third order shear deformation plate theory further relaxes the kinematic hypothesis by removing the straightness assumption; i.e., the straight normal to the middle plane before deformation may become cubic curves after deformation. The most significant difference between the classical and shear deformation theories is the effect of including transverse shear deformation on the predicted deflections, frequencies, and buckling loads [19].

A unified derivation of various shear-deformation models consists of Kirchhoff-Love type, Mindlin-Reissner type theory, third order theory, Layer-Wise theory and Exact-Solution. Librescu et al. [22] studied the correlation between two apparently different higher-order theories and First order transverse shear deformation theory (FSDT) of anisotropic plates. The Kirchhoff-Love assumptions were developed by Librescu and Schmidt [23]. The theory incorporates normal and shear deformation (transverse) as well as the higher-order effects, and accounts for small strains and moderate rotations of the normal.

For experimental work, shear deformation validation and compared structural theories, Stoffle [20] measured and simulated vibrations of viscoplastic plates under impulsive loading and determined how accurately the measured deformations can be calculated by the chosen constitutive and structural theories. He assumed a first-order shear deformation shell theory and applied small strains and moderate rotations and viscoplastic laws. He applied short time measurement techniques to shock tubes in order to record fast loading processes and plate deformations.

As mentioned above, shear deformation theories have been applied to consider transverse shear strains and rotation. Axisymmetric bending and stretching of functionally graded solid circular and annular plates were studied using the second-order shear deformation plate theory by Saidi and Sahraee [21]. Khdeir and Reddy [17] studied the free vibration of laminated composite plates using SSDT. Bahtuei and Eslami [18] also investigated the coupled thermoelastic response of a FG circular cylindrical shell by considering SSDT.

To the authors' knowledge, not much work has been done in the area of the dynamic stability of FG plate by using SSDT. In this study, the free vibration of FG plates (rectangular and square) by using SSDT is presented. The material properties of the plates are graded along the thickness direction according to a volume fraction power law distribution. Classical elasticity is considered and the complete governing equations are presented. Navier's method is applied to solve the equations. This work aims to investigate the effect of some basic factors such as material properties, side-to-side and side-to-thickness ratio for FG quadrangular plates on simply supported boundary conditions.

2. Gradation relations

The most commonly used models for most of the literature that express the variation of material properties in FGMs is the power law distribution of the volume fraction. According

to this model, the material property gradation through the thickness of the plate is assumed to be in the following form [10]:

$$E = E(x_3) = (E_c - E_m)(x_3 / h + 1/2)^p + E_m \tag{1a}$$

$$\rho = \rho(x_3) = (\rho_c - \rho_m)(x_3 / h + 1/2)^p + \rho_m \tag{1b}$$

Here E and ρ denote the modulus of elasticity and density of FG structure, while the parameters with subscript m or c represent the material properties of a pure metal and pure ceramic plate, respectively. The thickness coordinate variable is presented by x_3 while $-\frac{h}{2} \le x_3 \le \frac{h}{2}$, where h is the total thickness of the plate as shown in Figure 1. $p \ge 0$ is the volume fraction exponent (also called grading index in this paper); $(x_3 / h + 1/2)^p$ denotes the volume fraction of the ceramic.

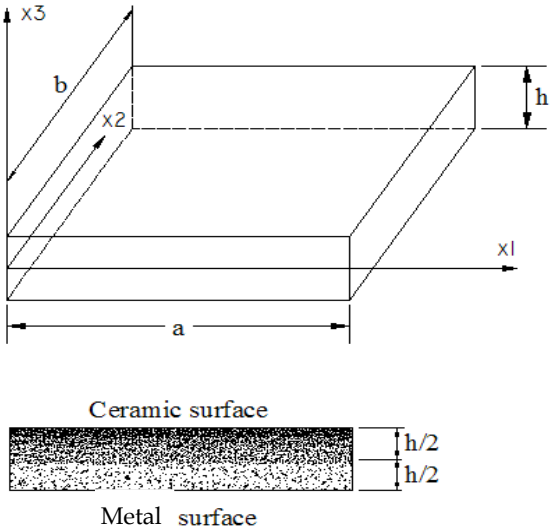

Fig. 1. Functionally graded plate.

A FG rectangular is considered as shown in Figure 1. The material in the top surface and in the bottom surface is Full-Ceramic and Full-Metal respectively, and between these two pure materials, the power law distribution of material is applied. The most well-known FGM is compositionally graded from a ceramic to a metal to incorporate such diverse properties as heat, wear and oxidation resistance of ceramics with the toughness, strength, machinability and bending capability of metals [7].

3. Elastic equations

Under consideration is a thin FG plate with constant thickness h, width, a, and length, b, as shown in Figure 1. Cartesian coordinate system (x_1, x_2, x_3) is used.

3.1 Displacement field and strains

The SSDT is based on the following representation of the displacement field:

$$u_1 = u + x_3\phi_1 + x_3^2\phi_2 \tag{2a}$$

$$u_2 = v + x_3\psi_1 + x_3^2\psi_2 \tag{2b}$$

$$u_3 = w \tag{2c}$$

Where (u_1, u_2, u_3) denote the displacement components in the (x_1, x_2, x_3) directions respectively; (u, v, w) are the displacements of a point on the mid plane $(x_1, x_2, 0)$. All displacement components $(u, v, w, \phi_1, \phi_2, \psi_1, \psi_2)$ are functions of position (x_1, x_2) and time t. The strain-displacement equations of the linear strain are given by [19].

$$\begin{Bmatrix} \varepsilon_{11} \\ \varepsilon_{22} \\ \gamma_{12} \end{Bmatrix} = \begin{Bmatrix} \varepsilon_{11}^0 \\ \varepsilon_{22}^0 \\ \varepsilon_{12}^0 \end{Bmatrix} + x_3 \begin{Bmatrix} \kappa_{11} \\ \kappa_{22} \\ \kappa_{12} \end{Bmatrix} + x_3^2 \begin{Bmatrix} \kappa_{11}' \\ \kappa_{22}' \\ \kappa_{12}' \end{Bmatrix} \tag{3a}$$

$$\begin{Bmatrix} \gamma_{23} \\ \gamma_{13} \end{Bmatrix} = \begin{Bmatrix} \gamma_{23}^0 \\ \gamma_{13}^0 \end{Bmatrix} + x_3 \begin{Bmatrix} \gamma_{23}^1 \\ \gamma_{13}^1 \end{Bmatrix} \tag{3b}$$

where

$$\begin{aligned}
&\varepsilon_{11}^0 = \frac{\partial u}{\partial x_1}, \kappa_{11} = \frac{\partial \phi_1}{\partial x_1}, \kappa_{11}' = \frac{\partial \phi_2}{\partial x_1} \\
&\varepsilon_{22}^0 = \frac{\partial v}{\partial x_2}, \kappa_{22} = \frac{\partial \psi_1}{\partial x_2}, \kappa_{22}' = \frac{\partial \psi_2}{\partial x_2} \\
&\varepsilon_{12}^0 = \frac{\partial u}{\partial x_2} + \frac{\partial v}{\partial x_1}, \kappa_{12} = \frac{\partial \phi_1}{\partial x_2} + \frac{\partial \psi_1}{\partial x_1}, \kappa_{12}' = \frac{\partial \phi_2}{\partial x_2} + \frac{\partial \psi_2}{\partial x_1} \\
&\gamma_{23}^0 = \psi_1 + \frac{\partial w}{\partial x_2}, \gamma_{13}^0 = \phi_1 + \frac{\partial w}{\partial x_1}, \gamma_{23}^1 = 2\psi_2, \gamma_{13}^1 = 2\phi_2
\end{aligned} \tag{4}$$

3.2 Stress-strain relations

The stress-strain relations are given by [17, 19].

$$\begin{Bmatrix} \sigma_{11} \\ \sigma_{22} \\ \sigma_{23} \\ \sigma_{13} \\ \sigma_{12} \end{Bmatrix} = \begin{Bmatrix} q_{11} & q_{12} & 0 & 0 & 0 \\ q_{12} & q_{22} & 0 & 0 & 0 \\ 0 & 0 & q_{44} & 0 & 0 \\ 0 & 0 & 0 & q_{55} & 0 \\ 0 & 0 & 0 & 0 & q_{66} \end{Bmatrix} \begin{Bmatrix} \varepsilon_{11} \\ \varepsilon_{22} \\ \gamma_{23} \\ \gamma_{13} \\ \gamma_{12} \end{Bmatrix} \tag{5}$$

where q_{ij} are the material constants given by

$$q_{11}=q_{22}=\frac{E}{1-\nu^2} \qquad q_{12}=\nu q_{11} \qquad q_{44}=q_{55}=q_{66}=\frac{E}{2(1+\nu)} \tag{6}$$

Hence, it follows that

$$\begin{Bmatrix}\sigma_{11}\\ \sigma_{22}\\ \sigma_{23}\\ \sigma_{13}\\ \sigma_{12}\end{Bmatrix}=\begin{bmatrix}q_{11} & q_{12} & 0 & 0 & 0\\ q_{12} & q_{22} & 0 & 0 & 0\\ 0 & 0 & q_{66} & 0 & 0\\ 0 & 0 & 0 & q_{55} & 0\\ 0 & 0 & 0 & 0 & q_{44}\end{bmatrix}\left(\begin{Bmatrix}\varepsilon_{11}^0\\ \varepsilon_{22}^0\\ \gamma_{23}^0\\ \gamma_{13}^0\\ \varepsilon_{12}^0\end{Bmatrix}+x_3\begin{Bmatrix}\kappa_{11}\\ \kappa_{22}\\ \gamma_{23}^1\\ \gamma_{13}^1\\ \kappa_{12}\end{Bmatrix}+x_3^2\begin{Bmatrix}\kappa_{11}^{'}\\ \kappa_{22}^{'}\\ 0\\ 0\\ \kappa_{12}^{'}\end{Bmatrix}\right) \tag{7}$$

3.3 Equations of motion

For the case of a rectangular plate, K, U and V are the kinetic, strain and potential energies of the body, respectively. The summation of the potential energy of external forces and strain energy, $U+V$, is the total potential energy, Π, of the body. Hamilton's principle for an elastic body is given by,

$$\int_{t_1}^{t_2}\left(\delta K-\delta\Pi\right)dt=0 \tag{8}$$

The inertias are defined by

$$I_i=\int_{\frac{-h}{2}}^{\frac{h}{2}}\rho_0\left(x_3\right)^i dx_3 \qquad \left(i=0,1,2,...,6\right) \tag{9}$$

Hamilton's principle, equation (8), along with the SSDT, given by equation (2), yields the complete form of the equilibrium equations:

$$\begin{aligned}
&\frac{\partial Q_{13}}{\partial x_1}+\frac{\partial Q_{23}}{\partial x_2}=I_0\ddot{w}\\
&\frac{\partial M_{11}}{\partial x_1}+\frac{\partial M_{12}}{\partial x_2}-Q_{13}=I_2\ddot{\phi}_1+I_1\ddot{u}+I_3\ddot{\phi}_2\\
&\frac{\partial L_{11}}{\partial x_1}+\frac{\partial L_{12}}{\partial x_2}-2R_{13}=I_2\ddot{u}+I_4\ddot{\phi}_2+I_3\ddot{\phi}_1\\
&\frac{\partial M_{22}}{\partial x_2}+\frac{\partial M_{12}}{\partial x_1}-Q_{23}=I_2\ddot{\psi}_1+I_1\ddot{v}+I_3\ddot{\psi}_2\\
&\frac{\partial L_{22}}{\partial x_2}+\frac{\partial L_{12}}{\partial x_1}-2R_{23}=I_2\ddot{v}+I_4\ddot{\psi}_2+I_3\ddot{\psi}_1
\end{aligned} \tag{10}$$

where N, M, L, Q and R are the stress resultants. These parameters can be represented by

$$\begin{Bmatrix} N_{11} \\ N_{22} \\ N_{12} \end{Bmatrix} = \int_{\frac{-h}{2}}^{\frac{h}{2}} \begin{Bmatrix} \sigma_{11} \\ \sigma_{22} \\ \sigma_{12} \end{Bmatrix} dx_3 \quad \begin{Bmatrix} N_{11} \\ N_{22} \\ N_{12} \end{Bmatrix} = \begin{bmatrix} A_{11}\varepsilon_{11}^0 + B_{11}\kappa_{11} + D_{11}\kappa_{11}^{'} + A_{12}\varepsilon_{22}^0 + B_{12}\kappa_{22} + D_{12}\kappa_{22}^{'} \\ A_{12}\varepsilon_{11}^0 + B_{12}\kappa_{11} + D_{12}\kappa_{11}^{'} + A_{22}\varepsilon_{22}^0 + B_{22}\kappa_{22} + D_{22}\kappa_{22}^{'} \\ A_{66}\varepsilon_{12}^0 + B_{66}\kappa_{12} + D_{66}\kappa_{12}^{'} \end{bmatrix} \quad (11a)$$

$$\begin{Bmatrix} M_{11} \\ M_{22} \\ M_{12} \end{Bmatrix} = \int_{\frac{-h}{2}}^{\frac{h}{2}} \begin{Bmatrix} \sigma_{11} \\ \sigma_{22} \\ \sigma_{12} \end{Bmatrix} x_3 dx_3 \quad \begin{Bmatrix} M_{11} \\ M_{22} \\ M_{12} \end{Bmatrix} = \begin{bmatrix} B_{11}\varepsilon_{11}^0 + D_{11}\kappa_{11} + E_{11}\kappa_{11}^{'} + B_{12}\varepsilon_{22}^0 + D_{12}\kappa_{22} + E_{12}\kappa_{22}^{'} \\ B_{12}\varepsilon_{11}^0 + D_{12}\kappa_{11} + E_{12}\kappa_{11}^{'} + B_{22}\varepsilon_{22}^0 + D_{22}\kappa_{22} + E_{22}\kappa_{22}^{'} \\ B_{66}\varepsilon_{12}^0 + D_{66}\kappa_{12} + E_{66}\kappa_{12}^{'} \end{bmatrix} \quad (11b)$$

$$\begin{Bmatrix} L_{11} \\ L_{22} \\ L_{12} \end{Bmatrix} = \int_{\frac{-h}{2}}^{\frac{h}{2}} \begin{Bmatrix} \sigma_{11} \\ \sigma_{22} \\ \sigma_{12} \end{Bmatrix} x^2{}_3 dx_3 \quad \begin{Bmatrix} L_{11} \\ L_{22} \\ L_{12} \end{Bmatrix} = \begin{bmatrix} D_{11}\varepsilon_{11}^0 + E_{11}\kappa_{11} + F_{11}\kappa_{11}^{'} + D_{12}\varepsilon_{22}^0 + E_{12}\kappa_{22} + F_{12}\kappa_{22}^{'} \\ D_{12}\varepsilon_{11}^0 + E_{12}\kappa_{11} + F_{12}\kappa_{11}^{'} + D_{22}\varepsilon_{22}^0 + E_{22}\kappa_{22} + F_{22}\kappa_{22}^{'} \\ D_{66}\varepsilon_{12}^0 + E_{66}\kappa_{12} + F_{66}\kappa_{12}^{'} \end{bmatrix} \quad (11c)$$

$$\begin{Bmatrix} Q_{13} \\ Q_{23} \end{Bmatrix} = \int_{\frac{-h}{2}}^{\frac{h}{2}} \begin{Bmatrix} \sigma_{13} \\ \sigma_{23} \end{Bmatrix} dx_3 \,, \quad \begin{Bmatrix} Q_{13} \\ Q_{23} \end{Bmatrix} = \begin{bmatrix} A_{55}\gamma_{13}^0 + B_{55}\gamma_{13}^1 \\ A_{44}\gamma_{23}^0 + B_{44}\gamma_{23}^1 \end{bmatrix} \quad (11d)$$

$$\begin{Bmatrix} R_{13} \\ R_{23} \end{Bmatrix} = \int_{\frac{-h}{2}}^{\frac{h}{2}} \begin{Bmatrix} \sigma_{13} \\ \sigma_{23} \end{Bmatrix} x_3 dx_3 \,, \quad \begin{Bmatrix} R_{13} \\ R_{23} \end{Bmatrix} = \begin{bmatrix} B_{55}\gamma_{13}^0 + D_{55}\gamma_{13}^1 \\ B_{44}\gamma_{23}^0 + D_{44}\gamma_{23}^1 \end{bmatrix} \quad (11e)$$

where

$$A_{ij}, B_{ij}, D_{ij}, E_{ij}, F_{ij} = \int_{\frac{-h}{2}}^{\frac{h}{2}} q_{ij}\left(1, x_3, x_3^2, x_3^3, x_3^4\right) dx_3 \quad (12a)$$

Here $A_{ij}, B_{ij}, D_{ij}, E_{ij}$ *and* F_{ij} are the plate stiffnesses.

$$\text{For} \begin{cases} A_{ij}, D_{ij}, F_{ij} & (i, j = 1,2,4,5,6) \\ E_{ij}, B_{ij} & (i, j = 1,2,6) \end{cases} \quad (12b)$$

By substituting equation (4) into equation (11) and then into equation (10) and also by applying definition (12), Navier's equations for FG plates are obtained as follows:

$$\begin{aligned} &A_{11}\frac{\partial^2 u}{\partial x_1^2} + A_{66}\frac{\partial^2 u}{\partial x_2^2} + \left(A_{12} + A_{66}\right)\frac{\partial^2 v}{\partial x_1 \partial x_2} + B_{11}\frac{\partial^2 \phi_1}{\partial x_1^2} + B_{66}\frac{\partial^2 \phi_1}{\partial x_2^2} + D_{11}\frac{\partial^2 \phi_2}{\partial x_1^2} + \\ &D_{66}\frac{\partial^2 \phi_2}{\partial x_2^2} + \left(B_{12} + B_{66}\right)\frac{\partial^2 \psi_1}{\partial x_1 \partial x_2} + \left(D_{12} + D_{66}\right)\frac{\partial^2 \psi_2}{\partial x_1 \partial x_2} = I_0 \ddot{u} + I_2 \ddot{\phi}_2 + I_1 \ddot{\phi}_1 \end{aligned} \quad (13a)$$

$$A_{12}\frac{\partial^2 u}{\partial x_1 \partial x_2}+A_{66}\frac{\partial^2 u}{\partial x_1 \partial x_2}+A_{22}\frac{\partial^2 v}{\partial x_2^2}+A_{66}\frac{\partial^2 v}{\partial x_1^2}+(B_{12}+B_{66})\frac{\partial^2 \phi_1}{\partial x_1 \partial x_2}+(D_{12}+D_{66})\frac{\partial^2 \phi_2}{\partial x_1 \partial x_2}$$
$$+B_{66}\frac{\partial^2 \psi_1}{\partial x_1^2}+B_{22}\frac{\partial^2 \psi_1}{\partial x_2^2}+D_{66}\frac{\partial^2 \psi_2}{\partial x_1^2}+D_{22}\frac{\partial^2 \psi_2}{\partial x_2^2}=I_0\ddot{v}+I_2\ddot{\psi}_2+I_1\ddot{\psi}_1 \quad (13b)$$

$$A_{55}\frac{\partial \phi_1}{\partial x_1}+A_{55}\frac{\partial^2 w}{\partial {x_1}^2}+2B_{55}\frac{\partial \phi_2}{\partial x_1}+A_{44}\frac{\partial \psi_1}{\partial x_2}+A_{44}\frac{\partial^2 w}{\partial {x_2}^2}+2B_{44}\frac{\partial \psi_2}{\partial x_2}=I_0\ddot{w} \quad (13c)$$

$$B_{11}\frac{\partial^2 u}{\partial x_1^2}+B_{66}\frac{\partial^2 u}{\partial x_2^2}+(B_{12}+B_{66})\frac{\partial^2 v}{\partial x_1 \partial x_2}+D_{11}\frac{\partial^2 \phi_1}{\partial x_1^2}+D_{66}\frac{\partial^2 \phi_1}{\partial x_2^2}$$
$$+E_{11}\frac{\partial^2 \phi_2}{\partial x_1^2}+E_{66}\frac{\partial^2 \phi_2}{\partial x_2^2}+(D_{12}+D_{66})\frac{\partial^2 \psi_1}{\partial x_1 \partial x_2}+(E_{12}+E_{66})\frac{\partial^2 \psi_2}{\partial x_1 \partial x_2} \quad (13d)$$
$$-A_{55}\left(\frac{\partial w}{\partial x_1}\right)-A_{55}\phi_1-2B_{55}\phi_2=I_2\ddot{\phi}_1+I_1\ddot{u}+I_3\ddot{\phi}_2$$

$$D_{11}\frac{\partial^2 u}{\partial x_1^2}+D_{66}\frac{\partial^2 u}{\partial x_2^2}+(D_{12}+D_{66})\frac{\partial^2 v}{\partial x_1 \partial x_2}+E_{11}\frac{\partial^2 \phi_1}{\partial x_1^2}+E_{66}\frac{\partial^2 \phi_1}{\partial x_2^2}+F_{11}\frac{\partial^2 \phi_2}{\partial x_1^2}+F_{66}\frac{\partial^2 \phi_2}{\partial x_2^2}$$
$$+(E_{12}+E_{66})\frac{\partial^2 \psi_1}{\partial x_1 \partial x_2}+(F_{12}+F_{66})\frac{\partial^2 \psi_2}{\partial x_1 \partial x_2}-2\left(B_{55}\left(\frac{\partial w}{\partial x_1}\right)+2D_{55}\phi_2+B_{55}\phi_1\right) \quad (13e)$$
$$=I_2\ddot{u}+I_4\ddot{\phi}_2+I_3\ddot{\phi}_1$$

$$(B_{12}+B_{66})\frac{\partial^2 u}{\partial x_1 \partial x_2}+B_{22}\frac{\partial^2 v}{\partial x_2^2}+B_{66}\frac{\partial^2 v}{\partial x_1^2}-A_{44}\frac{\partial w}{\partial x_2}+(D_{12}+D_{66})\frac{\partial^2 \phi_1}{\partial x_1 \partial x_2}+$$
$$(E_{12}+E_{66})\frac{\partial^2 \phi_2}{\partial x_1 \partial x_2}+D_{66}\frac{\partial^2 \psi_1}{\partial x_1^2}+D_{22}\frac{\partial^2 \psi_1}{\partial x_2^2}+E_{66}\frac{\partial^2 \psi_2}{\partial x_1^2}+E_{22}\frac{\partial^2 \psi_2}{\partial x_2^2} \quad (13f)$$
$$-A_{44}\psi_1-2B_{44}\psi_2=I_2\ddot{\psi}_1+I_1\ddot{v}+I_3\ddot{\psi}_2$$

$$(D_{12}+D_{66})\frac{\partial^2 u}{\partial x_1 \partial x_2}+D_{66}\frac{\partial^2 v}{\partial x_1^2}+D_{22}\frac{\partial^2 v}{\partial x_2^2}-2B_{44}\frac{\partial w}{\partial x_2}+(E_{12}+E_{66})\frac{\partial^2 \phi_1}{\partial x_1 \partial x_2}$$
$$+(F_{12}+F_{66})\frac{\partial^2 \phi_2}{\partial x_1 \partial x_2}+E_{66}\frac{\partial^2 \psi_1}{\partial x_1^2}+E_{22}\frac{\partial^2 \psi_1}{\partial x_2^2}+F_{66}\frac{\partial^2 \psi_2}{\partial x_1^2}+F_{22}\frac{\partial^2 \psi_2}{\partial x_2^2} \quad (13g)$$
$$-2B_{44}\psi_1-4D_{44}\psi_2=I_2\ddot{v}+I_4\ddot{\psi}_2+I_3\ddot{\psi}_1$$

It can be noted by considering zero values for ϕ_2 & ψ_2 in equations (10) and (13), the FSDT equations can be obtained [19].

4. Boundary conditions

For the case of simply supported boundary conditions of FG, as shown in Figure 2, the following relations can be written:

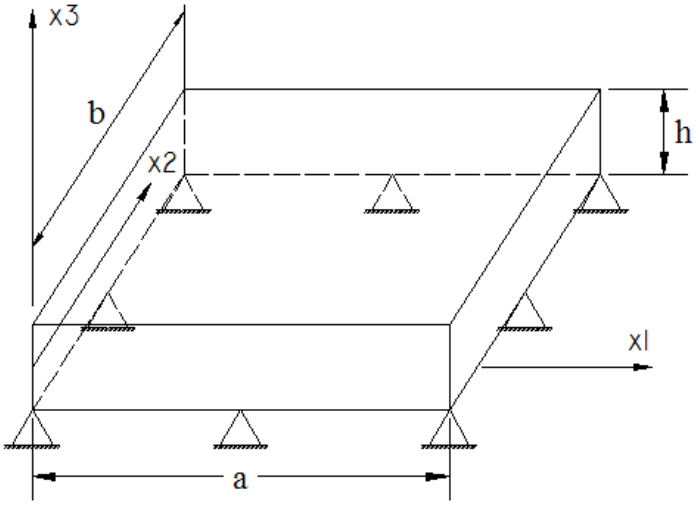

Fig. 2. Simply supported boundary condition in FG plates.

$$x_1 = 0, a \Rightarrow \begin{cases} v(0,x_2,t) = 0 \\ v(a,x_2,t) = 0 \\ \psi_1(0,x_2,t) = 0 \\ \psi_1(a,x_2,t) = 0 \\ \psi_2(0,x_2,t) = 0 \\ \psi_2(a,x_2,t) = 0 \end{cases}, \begin{cases} M_{11}(0,x_2,t) = 0 \\ N_{11}(0,x_2,t) = 0 \\ M_{11}(a,x_2,t) = 0 \\ N_{11}(a,x_2,t) = 0 \end{cases}, \begin{cases} w(0,x_2,t) = 0 \\ w(a,x_2,t) = 0 \end{cases} \tag{14a}$$

$$x_2 = 0, b \Rightarrow \begin{cases} u(x_1,0,t) = 0 \\ u(x_1,b,t) = 0 \\ \phi_1(x_1,0,t) = 0 \\ \phi_1(x_1,b,t) = 0 \\ \phi_2(x_1,0,t) = 0 \\ \phi_2(x_1,b,t) = 0 \end{cases}, \begin{cases} M_{22}(x_1,0,t) = 0 \\ N_{22}(x_1,0,t) = 0 \\ M_{22}(x_1,b,t) = 0 \\ N_{22}(x_1,b,t) = 0 \end{cases}, \begin{cases} w(x_1,0,t) = 0 \\ w(x_1,b,t) = 0 \end{cases} \tag{14b}$$

5. Method of solution

The Navier method is used for frequency analysis of a simply supported FG plate. The displacement field can be assumed to be given by:

$$u = \sum_{n=1}^{\infty} \sum_{m=1}^{\infty} u_{mn}(t) \cos \alpha x_1 \sin \beta x_2 \quad , u_{mn}(t) = U e^{-i\omega t} \tag{15a}$$

$$v = \sum_{n=1}^{\infty}\sum_{m=1}^{\infty} v_{mn}(t)\sin\alpha x_1 \cos\beta x_2 \quad , v_{mn}(t) = Ve^{-i\omega t} \tag{15b}$$

$$w = \sum_{n=1}^{\infty}\sum_{m=1}^{\infty} w_{mn}(t)\sin\alpha x_1 \sin\beta x_2 \quad , w_{mn}(t) = We^{-i\omega t} \tag{15c}$$

$$\phi_1 = \sum_{n=1}^{\infty}\sum_{m=1}^{\infty} \phi_{1mn}(t)\cos\alpha x_1 \sin\beta x_2 \quad , \phi_{1mn}(t) = \Phi_1 e^{-i\omega t} \tag{15d}$$

$$\phi_2 = \sum_{n=1}^{\infty}\sum_{m=1}^{\infty} \phi_{2mn}(t)\cos\alpha x_1 \sin\beta x_2 \quad , \phi_{2mn}(t) = \Phi_2 e^{-i\omega t} \tag{15e}$$

$$\psi_1 = \sum_{n=1}^{\infty}\sum_{m=1}^{\infty} \psi_{1mn}(t)\sin\alpha x_1 \cos\beta x_2 \quad , \psi_{1mn}(t) = \Psi_1 e^{-i\omega t} \tag{15f}$$

$$\psi_2 = \sum_{n=1}^{\infty}\sum_{m=1}^{\infty} \psi_{2mn}(t)\sin\alpha x_1 \cos\beta x_2 \quad , \psi_{2mn}(t) = \Psi_2 e^{-i\omega t} \tag{15g}$$

where

$$\alpha = \frac{m\pi}{a} \quad , \beta = \frac{n\pi}{b} \tag{16}$$

For natural vibrations, substituting equation (15) into the equations of motion (13), these equations reduce to the following forms:

$$[C]\begin{Bmatrix} U \\ V \\ W \\ \Phi_1 \\ \Phi_2 \\ \psi_1 \\ \psi_2 \end{Bmatrix} - \omega^2 [M]\begin{Bmatrix} U \\ V \\ W \\ \Phi_1 \\ \Phi_2 \\ \psi_1 \\ \psi_2 \end{Bmatrix} = \begin{Bmatrix} 0 \\ 0 \\ 0 \\ 0 \\ 0 \\ 0 \\ 0 \end{Bmatrix} \tag{17}$$

where ω is the natural frequency and

$$\begin{array}{lll}
C_{11} = A_{11}\alpha^2 + A_{66}\beta^2 & C_{21} = (A_{12} + A_{66})\alpha\beta & C_{31} = 0 \\
C_{12} = (A_{12} + A_{66})\alpha\beta & C_{22} = A_{66}\alpha^2 + A_{22}\beta^2 & C_{32} = 0 \\
C_{13} = 0 & C_{23} = 0 & C_{33} = A_{55}\alpha^2 + A_{44}\beta^2 \\
C_{14} = B_{11}\alpha^2 + B_{66}\beta^2 & , C_{24} = (B_{12} + B_{66})\alpha\beta & , C_{34} = A_{55}\alpha \\
C_{15} = D_{11}\alpha^2 + D_{66}\beta^2 & C_{25} = (D_{12} + D_{66})\alpha\beta & C_{35} = 2B_{55}\alpha \\
C_{16} = (B_{12} + B_{66})\alpha\beta & C_{26} = B_{66}\alpha^2 + B_{22}\beta^2 & C_{36} = A_{44}\beta \\
C_{17} = (D_{12} + D_{66})\alpha\beta & C_{27} = D_{66}\alpha^2 + D_{22}\beta^2 & C_{37} = 2B_{44}\beta
\end{array}$$

$$
\begin{aligned}
&C_{41} = B_{11}\alpha^2 + B_{66}\beta^2 && C_{51} = D_{11}\alpha^2 + D_{66}\beta^2 \\
&C_{42} = (B_{12} + B_{66})\alpha\beta && C_{52} = (D_{12} + D_{66})\alpha\beta \\
&C_{43} = A_{55}\alpha && C_{53} = 2B_{55}\alpha \\
&C_{44} = D_{11}\alpha^2 + D_{66}\beta^2 + A_{55}\ , && C_{54} = E_{11}\alpha^2 + E_{66}\beta^2 + 2B_{55}\ , \\
&C_{45} = E_{11}\alpha^2 + E_{66}\beta^2 + 2B_{55} && C_{55} = F_{11}\alpha^2 + F_{66}\beta^2 + 4D_{55} \\
&C_{46} = (D_{12} + D_{66})\alpha\beta && C_{56} = (E_{12} + E_{66})\alpha\beta \\
&C_{47} = (E_{12} + E_{66})\alpha\beta && C_{57} = (F_{12} + F_{66})\alpha\beta
\end{aligned}
$$

$$
\begin{aligned}
&C_{61} = (B_{12} + B_{66})\alpha\beta && C_{71} = (D_{12} + D_{66})\alpha\beta \\
&C_{62} = B_{66}\alpha^2 + B_{22}\beta^2 && C_{72} = D_{66}\alpha^2 + D_{22}\beta^2 \\
&C_{63} = A_{44}\beta && C_{73} = 2B_{44}\beta \\
&C_{64} = (D_{12} + D_{66})\alpha\beta && , C_{74} = (E_{12} + E_{66})\alpha\beta \\
&C_{65} = (E_{12} + E_{66})\alpha\beta && C_{75} = (F_{12} + F_{66})\alpha\beta \\
&C_{66} = D_{66}\alpha^2 + D_{22}\beta^2 + A_{44} && C_{76} = E_{66}\alpha^2 + E_{22}\beta^2 + 2B_{44} \\
&C_{67} = E_{66}\alpha^2 + E_{22}\beta^2 + 2B_{44} && C_{77} = F_{66}\alpha^2 + F_{22}\beta^2 + 4D_{44}
\end{aligned}
\tag{18}
$$

By considering relations (18), equation (17) can be written as:

$$\left|C_{ij} - M_{ij}\omega^2\right| = 0 \tag{19}$$

By solving equation (19) and considering appropriate values for n and m in equation (16) the fundamental frequency of a quadrangle FG plate can be obtained.

6. Validation and numerical results

6.1 Validation

The results obtained for a FG plate by applying SSDT are compared with the results obtained by using TSDT as in Ref [5] and the exact solution of [14]. The following non-dimensional fundamental frequencies in Table 1 and Table 2 are obtained by considering material properties the same as [5].

Results in Table 1 and Table 2 show that the values obtained by SSDT are greater than those from TSDT and the exact solution. This is due to the fact that the transverse shear and rotary inertia will have more of an effect on a thicker plate. For the thick plates considered in this

$h/a = 0.05$			$h/a = 0.1$			$h/a = 0.2$		
Present study	Ref. [5]	Exact [14]	Present study	Ref. [5]	Exact [14]	Present study	Ref. [5]	Exact [14]
0.0158	0.0147	0.0153	0.0621	0.0592	0.0596	0.2306	0.2188	0.2192

Table 1. Dimensionless fundamental frequency ($\bar{\omega} = \omega h\sqrt{\frac{\rho_m}{E_m}}$) of a simply supported square (Al/Zro_2) FG plate ($p = 1$).

case, there is insignificant difference between the result predicted by SSDT and TSDT; SSDT slightly over predicts frequencies. It can be seen that there are good agreements between our results and other results.

$p=2$			$p=3$			$p=5$		
Present study	Ref. [5]	Exact [14]	Present Study	Ref. [5]	Exact [14]	Present Study	Ref. [5]	Exact [14]
0.2292	0.2188	0.2197	0.2306	0.2202	0.2211	0.2324	0.2215	0.2225

Table 2. Dimensionless fundamental frequency ($\bar{\omega} = \omega h \sqrt{\frac{\rho_m}{E_m}}$) of a simply supported square (Al/Zro$_2$) FG Plate, thickness-to-side is: $h / a = 0.2$.

Material property	$E(Gpa)$	$\rho(Kg/m^3)$	ν
SUS 304, Metal	201.04	8166	0.33
Aluminum, Metal	68.9	2700	0.33
Zirconia, Ceramic	211.0	4500	0.33
Si_3N_4, Ceramic	348.43	2370	0.24

Table 3. Properties of materials used in the numerical example.

6.2 Numerical example

For numerical illustration of the free vibration of a quadrangle FG plate with Zirconia and silicon nitride as the upper-surface ceramic and aluminum and SUS 304 as the lower-surface metal are considered the same as [10]:

6.2.1 Results and discussion for the first ten modes in quadrangular FG plates

In the following Tables, free vibrations are presented in dimensionless form for square and rectangular FG plates.

Tables 4 and 5 show the dimensionless frequency in square (a=b) SUS 304/Si3N4, FG plates. It can be noted that for the same values of grading index P , the natural frequency increases with increasing mode. The effect of grading index can be shown by comparing the frequency value for the fixed value of mode and changing the values of grading index p . It can be seen that, the frequency decreases with the increase of the grading index due to the stiffness decreases from pure ceramic to pure metal.

Tables 6 and 7 show the dimensionless frequency in rectangular (b=2a) SUS 304/Si3N4, FG plates. The effect of grading index can be shown by comparing the frequency for the same value of mode and considering different values of grading index p as shown in Table 5. It is clearly visible that the frequency decreases with the increasing grading index, caused by the stiffness decreasing with increasing grading index. For the same value of p , it can be said that the natural frequency increases with increasing mode. By comparing Tables 6, 7 and 4, 5 it can be observed that for the same values of grading index and mode, the fundamental frequency in square FG plates are greater than those in rectangular FG plates and by

$m \times n$	mode	$p=0$	$p=0.5$	$p=1$	$p=2$	$p=4$	$p=6$	$p=8$	$p=10$
1x1	1	5.76	3.904	3.393	3.027	2.795	2.697	2.638	2.597
1x2	2	13.846	9.366	8.139	7.259	6.700	6.464	6.323	6.227
2x1	3	13.846	9.366	8.139	7.259	6.700	6.464	6.323	6.227
2x2	4	21.353	14.441	12.547	11.187	10.321	9.957	9.741	9.593
2x3	5	32.859	22.220	19.305	17.203	15.863	15.300	14.967	14.741
3x2	6	32.859	22.220	19.305	17.203	15.863	15.300	14.967	14.741
3x3	7	43.369	29.323	25.472	22.689	20.911	20.167	19.729	19.431
3x4	8	56.798	38.405	33.362	29.703	27.356	26.377	25.801	25.412
4x3	9	56.798	38.405	33.362	29.703	27.356	26.377	25.801	25.412
4x4	10	69.054	46.690	40.555	36.091	33.221	32.026	31.327	30.856

Table 4. Variation of the frequency parameter ($\varpi = \omega a^2 / h\sqrt{\rho_c / E_c}$) with the grading index (p) for square. $SUS\ 304 / Si_3N_4$ FG square plates ($a/h=10, a=b$).

$m \times n$	mode	$p=0$	$p=0.5$	$p=1$	$p=2$	$p=4$	$p=6$	$p=8$	$. p=10 .$
1x1	1	5.338	3.610	3.137	2.796	2.580	2.489	2.435	2.398
1x2	2	11.836	8.003	6.953	6.193	5.706	5.502	5.382	5.301
2x1	3	11.836	8.003	6.953	6.193	5.706	5.502	5.382	5.301
2x2	4	17.263	11.672	10.138	9.022	8.305	8.006	7.831	7.714
2x3	5	24.881	16.828	14.621	13.002	11.950	11.513	11.258	11.089
3x2	6	24.881	16.828	14.621	13.002	11.950	11.513	11.258	11.089
3x3	7	31.354	21.209	18.426	16.375	15.0343	14.477	14.156	13.943
3x4	8	39.180	26.508	23.041	20.471	18.770	18.062	17.656	17.388
4x3	9	39.180	26.508	23.041	20.471	18.770	18.062	17.656	17.388
4x4	10	46.020	31.141	27.067	24.036	22.020	21.181	20.702	20.387

Table 5. Variation of the frequency parameter ($\varpi = \omega a^2 / h\sqrt{\rho_c / E_c}$) with the grading index (p) for $SUS\ 304 / Si_3N_4$ FG square plates ($a/h=5, a=b$).

$m \times n$	mode	$p=0$	$p=0.5$	$p=1$	$. p=2 .$	$p=4$	$p=6$	$p=8$	$p=10$
1x1	1	3.461	2.341	2.034	1.814	1.674	1.616	1.580	1.556
1x2	2	5.338	3.610	3.137	2.796	2.580	2.489	2.435	2.39
2x1	3	10.334	6.984	6.065	5.402	4.980	4.804	4.700	
2x2	4	11.836	8.00	6.948	6.188	5.702	5.499	5.380	5.300
2x3	5	14.199	9.599	8.337	7.422	6.836	6.592	6.449	6.552
3x2	6	20.484	13.845	12.020	10.689	9.835	9.482	9.276	9.139
3x3	7	22.373	15.125	13.133	11.678	10.740	10.352	10.126	9.976
3x4	8	24.881	16.824	14.611	12.989	11.940	11.505	11.254	11.085
4x3	9	31.656	21.409	18.585	16.506	15.157	14.602	14.282	14.071
4x4	10	33.715	22.805	19.802	17.587	16.142	15.547	15.205	14.979

Table 6. Variation of the frequency parameter ($\varpi = \omega a^2 / h\sqrt{\rho_c / E_c}$) with the grading index (p) for $SUS\ 304 / Si_3N_4$ FG rectangular plate ($a/h=5, a=0.5\times b$).

$m \times n$	mode	$p=0$	$p=0.5$	$p=1$	$p=2$	$p=4$	$p=6$	$p=8$	$p=10$
1x1	1	3.645	2.467	2.144	1.913	1.766	1.704	1.667	1.642
1x2	2	5.769	3.904	3.393	3.027	2.795	2.697	2.638	2.597
2x1	3	11.885	8.039	6.986	6.231	5.752	5.549	5.429	5.346
2x2	4	13.846	9.365	8.138	7.258	6.699	6.463	6.323	6.227
2x3	5	17.037	11.523	10.012	8.928	8.239	7.949	7.776	7.658
3x2	6	26.092	17.640	15.325	13.659	12.600	12.156	11.893	11.713
3x3	7	28.958	19.578	17.008	15.158	13.981	13.487	13.195	12.995
3x4	8	32.859	22.215	19.299	17.197	15.858	15.297	14.965	14.739
4x3	9	43.873	29.653	25.754	22.937	21.142	20.393	19.951	19.652
4x4	10	47.344	32.002	27.794	24.715	22.809	21.999	21.522	21.199

Table 7. Variation of the frequency parameter ($\varpi = \omega a^2 / h\sqrt{\rho_c / E_c}$) with the grading index (p) for $SUS\,304 / Si_3N_4$ FG rectangular plate ($a/h=10$, $a=0.5\times b$).

increasing the side-to-thickness ratio, the frequency also increases. It is evident that the grading index and side-to-thickness ratio effects in frequency are more significant than the other conditions.

6.2.2 Results and discussion for the natural frequency in quadrangular FG (SUS 304/Si3N4) plates

Figures (3) and (4) illustrate the dimensionless frequency versus grading index (p), for different values of side-to-thickness ratio (a/h) and side-to-side ratio (b/a), respectively.

In Figure 3, the effect of grading index (p) and side-to-thickness ratio (a/h) on dimensionless fundamental frequency of FG (SUS 304/Si3N4) plate is shown. It can be seen that the frequency decreases with increasing grading index, due to degradation of stiffness by the metallic inclusion. It can be observed that the natural frequency is maximum for full-ceramic ($p=0.0$) and this value increases with the increase of the side-to-thickness ratio, since the stiffness of thin plates is more effectively than the thick plates. It is seen that for the values (p), for $0<p<2$ the slope is greater than other parts ($p>2$). It can be said that for side-to-thickness ratios greater than twenty ($a/h>20$), the frequencies will be similar for different values of grading index. It can be noted that the difference between frequencies in $a/h=5$ and $a/h=10$ are greater than differences of frequency between $a/h=10$ and other curves for the same values of grading index p. And also it can be concluded that for $a/h>20$, the difference between the frequencies is small for the same value of grading index.

The effect of grading index (p) and side-to-side ratio (b/a) on dimensionless fundamental frequency of FG (SUS 304/Si3N4) plate can be seen in figure 4. It can be noted that the frequency increases with the increase of the b/a since rectangular plates can be treated as a one-dimensional problem for example, beams or plate strips. It can be observed that the frequency is almost constant for different values of grading index.

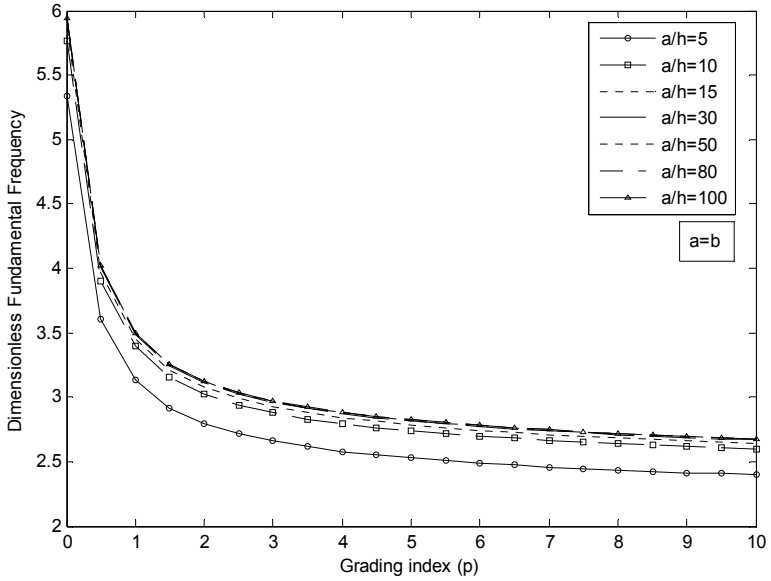

Fig. 3. Dimensionless frequency ($\varpi = \omega a^2 / h\sqrt{\rho_c / E_c}$) versus grading index (p) for different values of side-to-thickness ratio (a / h) in square ($b = a$) FG ($SUS\ 304 / Si_3N_4$) plates.

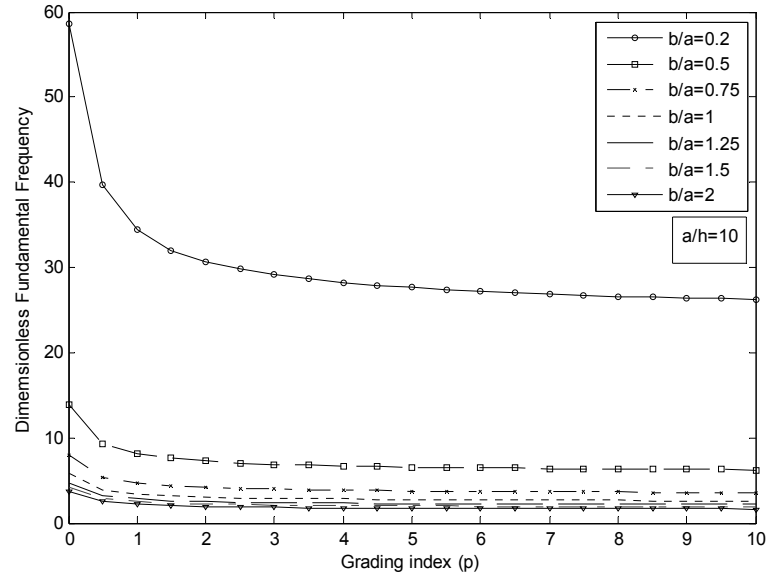

Fig. 4. Dimensionless frequency ($\varpi = \omega a^2 / h\sqrt{\rho_c / E_c}$) versus grading index (p) for different values of side-to-side ratio (b / a) FG ($SUS\ 304 / Si_3N_4$) plates when $a / h = 10.0$

Figures (5) and (6) show variation of dimensionless fundamental frequency of FG (SUS 304/Si3N4) plate with side-to-thickness ratio (a/h), for different values of grading index (p) and side-to side ratio (b/a), respectively.

It is seen from figure 5, the fundamental frequency increases with the increase of the value of side-to-thickness ratio (a/h). It is shown that the frequency decreases with the increase of the values of side-to-side (b/a). It can be noted that the slope of frequency versus side-to-thickness ratio (a/h) for part $5 < a/h < 10$ is greater than those in another part ($a/h > 10$).

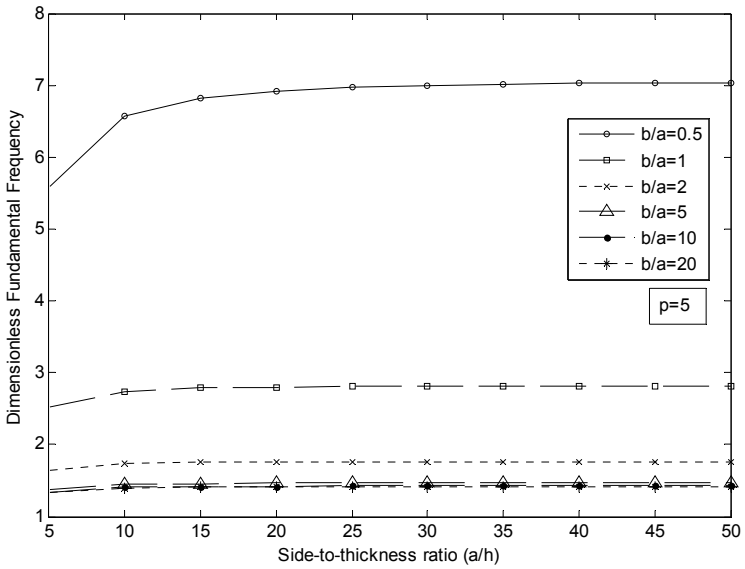

Fig. 5. Dimensionless frequency ($\varpi = \omega a^2 / h\sqrt{\rho_c / E_c}$) versus side-to-thickness ratio (a/h)for different values of side-to-side ratio (b/a) FG ($SUS\ 304 / Si_3N_4$) plates when $p = 5$.

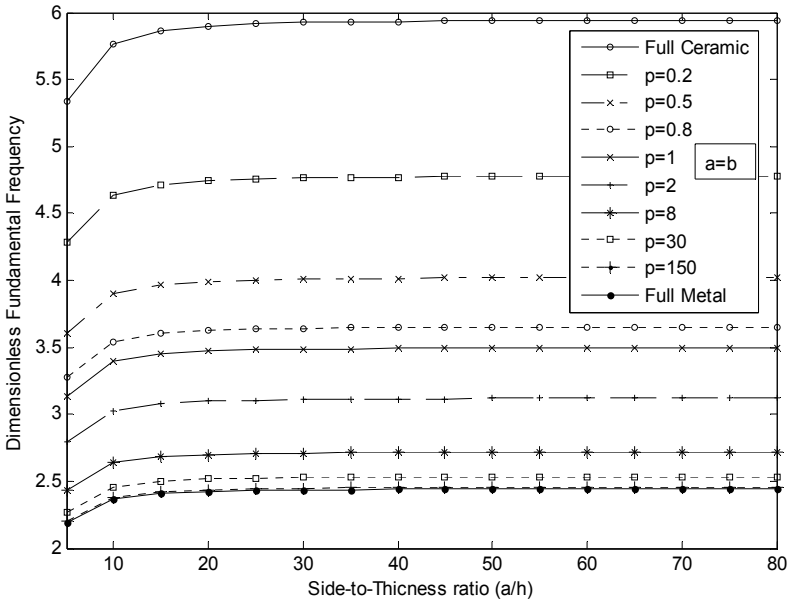

Fig. 6. Dimensionless frequency ($\varpi = \omega a^2 / h\sqrt{\rho_c / E_c}$) versus side-to-thickness ratio (a / h) for different values of grading index (p) in square ($b = a$) FG ($SUS\ 304 / Si_3N_4$) plates.

The variation of frequency with side-to-thickness ratio (a / h) for different values of grading index (p) is presented in Figure 6. As expected, by increasing the value of grading index (p) the values of frequency decrease due to the decrease in stiffness. Similarly, in figure (5) while the $5 < a / h < 10$, the slope is greater than another ratios. It can be noted that for the values of grading index $p > 30$, the results for frequency are similar.

Figures 7 and 8 present the variation of dimensionless frequency of FG (SUS 304/Si3N4) plate versus side-to-side ratio (b / a) for different values of grading index (p) and side-to-thickness ratio (a / h) , respectively.

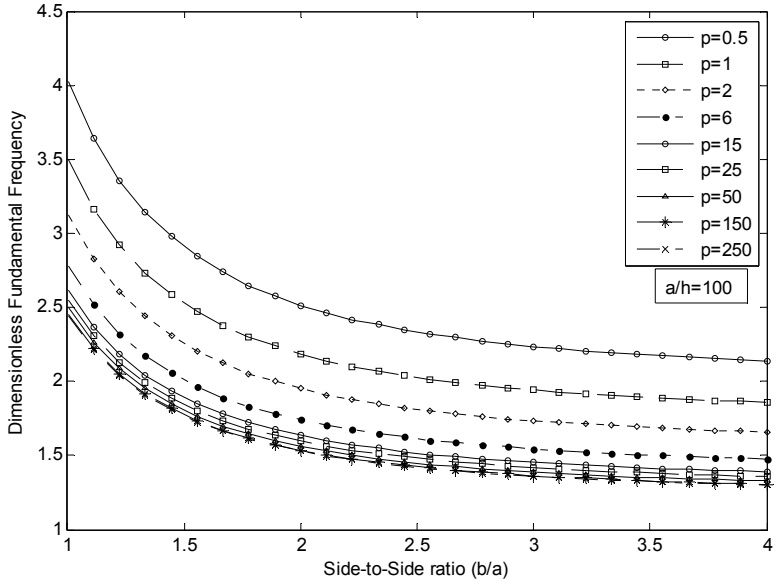

Fig. 7. Dimensionless frequency ($\varpi = \omega a^2 / h\sqrt{\rho_c / E_c}$) versus side-to-side ratio ($b = a$) for different values of grading index (p) FG ($SUS\ 304 / Si_3N_4$) plates when $a / h = 100$.

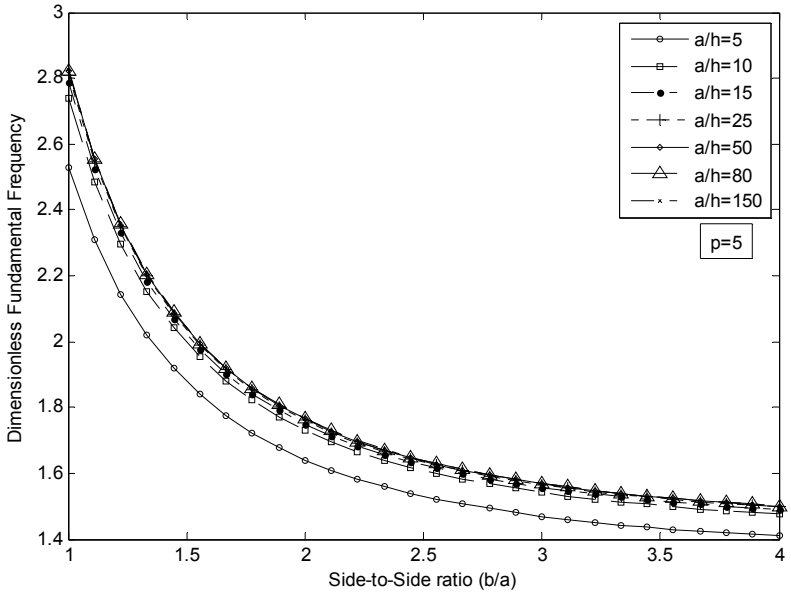

Fig. 8. Dimensionless frequency ($\varpi = \omega a^2 / h\sqrt{\rho_c / E_c}$) versus side-to-side ratio (b / a) for different values of side-to-thickness ratio (a / h) FG ($SUS\ 304 / Si_3N_4$) plates when $p = 5$.

In figure 7, it is shown that the frequency decreases with the increase of the value of side-to-side ratio (b/a) for all values of grading index (p). It is seen that the frequencies for FG quadrangular plates are between that of a full-ceramic plate and full-metal plate. As expected the frequencies in a full-ceramic plate are greater than those in a full-metal plate.
The results for dimensionless frequency versus side-to-side ratio (b/a) for different values of side-to-thickness ratio (a/h) in FG plate while grading index $p=5$ are shown in figure 8. It is seen that by increasing the value of b/a, the frequency decreases for all values of a/h. It can be noted for $a/h>10$ the results are similar.

7. Conclusions

In this chapter, free vibration of FG quadrangular plates were investigated thoroughly by adopting Second order Shear Deformation Theory (SSDT). It was assumed that the elastic properties of a FG quadrangular plate varied along its thickness according to a power law distribution. Zirconia and Si3N4 were considered as a ceramic in the upper surface while aluminum and SUS304 were considered as metals for the lower surface. The complete equations of motion were presented using Hamilton's principle. The equations were solved by using Navier's Method for simply supported FG plates.
Some general observations of this study can be deduced here:

- The decreasing slope of the fundamental frequency for $0<p<2$, is greater than another part ($p>2$) for all values of side-to-thickness ratio (a/h) in square FG plate.
- It was found that the fundamental frequency of the FG plate increases with the increase of the value of side-to-side ratio (b/a).
- For FG plates, the slope of increasing frequency versus side-to-thickness (a/h) when $5<a/h<10$ is greater than another part $(a/h>10)$ for any value of grading index and side-to-side ratio.
- The fundamental frequency versus side-to-side ratio (b/a) for FG quadrangular plates are between those of a full-ceramic plate and full-metal plate when $a/h=10$.

From the numerical results presented here, it can be proposed that the gradations of the constitutive components are the significant parameter in the frequency of quadrangular FG plates.

8. Acknowledgement

The authors would like to thank Universiti Putra Malaysia for providing the research grant (FRGS 07-10-07-398SFR 5523398) for this research work.

9. References

[1] Reddy JN. Analysis of functionally graded plates. Int. J. Numer Meth Eng 2000;47:663-684.
[2] Suresh S, Mortensen A. Fundamentals of functionally graded materials. London: IOM Communications Limited, 1998.
[3] Praveen GN, Reddy JN. Nonlinear transient thermoelastic analysis of functionally graded ceramic-metal plates. Int. J. Solids Struct 1998;35(33):4457-4476.

[4] Ng TY, Lam KY, Liew KM. Effects of FGM materials on the parametric resonance of plate structure. Comput. Meth Appl. Mech. Eng 2000;190:953-962.
[5] Ferreira AJM, Batra RC, Roque CMC, Qian LF, Jorge RMN. Natural frequencies of functionally graded plates by a meshless method. Comp Struct 2006;75:593–600.
[6] Woo J, Meguid SA, Ong LS. Nonlinear free vibration behavior of functionally graded plates. J. Sound Vibr 2006;289:595–611.
[7] Zhao X, Lee YY, Liew KM. Free vibration analysis of functionally graded plates using the element-free kp-Ritz method. J. Sound Vibr 2008.
[8] Batra RC, Jin J. Natural frequencies of a functionally graded anisotropic rectangular plate. J. Sound Vibr 2005;282:509–516.
[9] Batra RC, Aimmanee S. Vibrations of thick isotropic plates with higher order shear and normal deformable plate theories. Comput Struct 2005;83:934–955.
[10] Bayat M, Saleem M, Sahari BB, Hamouda AMS, Mahdi E. Thermo elastic analysis of a functionally graded rotating disk with small and large deflections. Thin-Walled Struct 2007;45:677–691.
[11] Bayat M, Sahari BB, Saleem M, Ali A, Wong SV. Thermo elastic solution of a functionally graded variable thickness rotating disk with bending based on the first-order shear deformation theory. Thin-Walled Struct 2008.
[12] Heidary F, M. Reza Eslami MR. Piezo-control of forced vibrations of a thermoelastic composite plate. Comp Struct 2006;74(1):99-105
[13] Cheng ZQ, Batra RC. 2000, exact correspondence between eigenvalue of membranes and functionally graded simply supported polygonal plates. J. Sound Vibr 2000;229(4):879-895.
[14] Vel SS, Batra RC. Three-dimensional exact solution for the vibration of functionally graded rectangular plates. J. Sound Vibr 2004;272: 703-30.
[15] Huang XL, Shen H. Nonlinear vibration and dynamic response of functionally graded plates in thermal environments. Int J. Solids Struct 2004;41:2403–2427.
[16] Ferreira AJM., Batra RC, Roque CMC, Qian LF, Martins PALS. Static analysis of functionally graded plates using third-order shear deformation theory and meshless method. Comp Struct 2005;69:449–457.
[17] Khdeir AA, Reddy JN. Free vibrations of laminated composite plates using second-order shear deformation theory. Comp Struct 1999;71:617-626.
[18] Bahtui A, Eslami MR. Coupled thermoelasticity of functionally graded cylindrical shells. Mech Res Commun 2007; 34(1):1-18.
[19] Reddy JN. Theory and Analysis of Elastic Plates and Shells. New York: CRC Press; 2007.
[20] Stoffel, M. (2005). Experimental validation of simulated plate deformations caused by shock waves, Math. Mech., 85(9):643 – 659.
[21] Saidi Ali Reza, Sahraee Shahab, (2006). Axisymmetric solutions of functionally graded circular and annular plates using second-order shear deformation plate theory, ESDA2006-95699, 8th Biennial ASME Conference on Engineering Systems Design and Analysis, Torino, Italy.

[22] Librescu,L., Khdeir, A.A., Reddy, J.N. (1987). Comprehensive Analysis of the State of Stressof Elastic Anisotropie Flat Plates Using Refined Theories, *Acta* Mechanica, 70:57-81.

[23] Librescu, L., Schmidt, R. (1988).Refined Theories of Elastic Anisotropic Shell Accounting for Small Strain and Moderate Rotations, Int. J. Non-Linear Mechanics, 23(3):217-229.

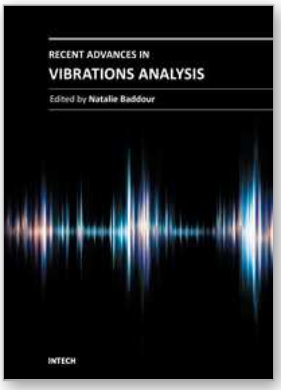

Recent Advances in Vibrations Analysis
Edited by Dr. Natalie Baddour

ISBN 978-953-307-696-6
Hard cover, 236 pages
Publisher InTech
Published online 09, September, 2011
Published in print edition September, 2011

This book covers recent advances in modern vibrations analysis, from analytical methods to applications of vibrations analysis to condition monitoring. Covered topics include stochastic finite element approaches, wave theories for distributed parameter systems, second other shear deformation theory and applications of phase space to the identifications of nonlinearities and transients. Chapters on novel condition monitoring approaches for reducers, transformers and low earth orbit satellites are included. Additionally, the book includes chapters on modelling and analysis of various complex mechanical systems such as eccentric building systems and the structural modelling of large container ships.

InTech Europe
University Campus STeP Ri
Slavka Krautzeka 83/A
51000 Rijeka, Croatia
Phone: +385 (51) 770 447
Fax: +385 (51) 686 166
www.intechopen.com

InTech China
Unit 405, Office Block, Hotel Equatorial Shanghai
No.65, Yan An Road (West), Shanghai, 200040, China
中国上海市延安西路65号上海国际贵都大饭店办公楼405单元
Phone: +86-21-62489820
Fax: +86-21-62489821